Schneider, T., H. Weber, J. Franke, and S. Brönnimann (2013) The Storm Surge Event of the Netherlands in 1953. In: Brönnimann, S. and O. Martius (Eds.) *Weather extremes during the past 140 years*. Geographica Bernensia G89, p. 35-43, DOI: 10.4480/GB2013.G89.04.

The Storm Surge Event of the Netherlands in 1953

Tobias Schneider, Helga Weber, Jörg Franke, and Stefan Brönnimann*

Oeschger Centre for Climate Change Research and Institute of Geography, University of Bern, Switzerland

Abstract

A disastrous storm surge hit the coast of the Netherlands on 31 January and 1 February 1953. We examine the meteorological situation during this event using the Twentieth Century Reanalysis (20CR) data set. We find a strong pressure gradient between Ireland and northern Germany accompanied by strong north-westerly winds over the North Sea. Storm driven sea level rise combined with spring tide contributed to this extreme event. The state of the atmosphere in 20CR during this extreme event is in good agreement with historical observational data.

1. Introduction

Storm surges are a major risk at the coast of the Netherlands which was highlighted by the magnitude of the storm surge in the year 1953. From Saturday, 31 January 1953 to Sunday, 1 February 1953, a storm surge "raged across the northwest European shelf" (Gerritsen, 2005). Many dikes could not withstand the enormous water pressure and began to burst almost simultaneously (Jung et al., 2004). Several polders were inundated followed by severe losses of human lives and damages of land and property. Figure 1 shows the damage viewed from a helicopter flying over the affected area.

The Holland storm surge of 1953, which occurred at night, surprised many people in their sleep (Gerritsen, 2005). As a consequence, over 1800 people were killed (Wolf and Flather, 2005), 1350 km^2 of land were inundated (Verlaan et al., 2005), and over one thousand farms were destroyed (Jung et al., 2004). Although, according to Rossiter (1954), even higher water levels had occurred previously, the storm surge had a catastrophic impact.

* Corresponding author: Stefan Brönnimann, University of Bern, Institute of Geography, Hallerstr. 12, CH-3012 Bern, Switzerland. E-mail: stefan.broennimann@giub.unibe.ch

Figure 1. Viewed from a U.S. Army helicopter, a Zuid Beveland town gives a hint of the tremendous damage wrought by the flood to Dutch islands. Source: National Archives and Records Administration (NARA), ARC Identifier 541705.

Following Rossiter (1954), Hansen (1956), Jung et al. (2004), Gerritsen (2005), and Wolf and Flather (2005), the catastrophic impact of the storm surge was due to the combination of the high wind speed and the spring tide. The high wind speeds were associated with a cyclone over the North Sea, which brought gale force wind from north and northwesterly direction. Due to the track of the storm, the strong winds blew over shallow areas of the western and southern North Sea for a rather long time, pushing large volumes of water southward (Gerritsen, 2005). Large wind waves occurred due to the meridional elongation of the windstorm area across the North Sea, resulting in a long fetch (Wolf and Flather, 2005). Understanding both the oceanic (tidal) and atmospheric (meteorological) processes of this past event is relevant with respect to disaster prevention in a future, altered climate.

The storm surge on 31 January and 1 February 1953 was well studied by many authors. Although many studies focused not directly on the meteorological causes, but on the importance of awareness and preparedness (Gerritsen, 2005) or predictability (Jung et al., 2004), the storm is well studied using various data sets (*e.g.,* McRobie et al., 2005; Smits et al., 2005; Verlaan et al., 2005; Wolf and Flather, 2005). Jung et al. (2004), for instance, used two versions of the data assimilation system of the European Centre for Medium-Range Weather Forecasts (ECWMF) Integrated Forecasting System (IFS) to carry out reanalyses of this and other storm events. This makes the Holland storm 1953 an ideal case for investigating the applicability of the "Twentieth Century Reanalysis" (20CR, Compo et al.

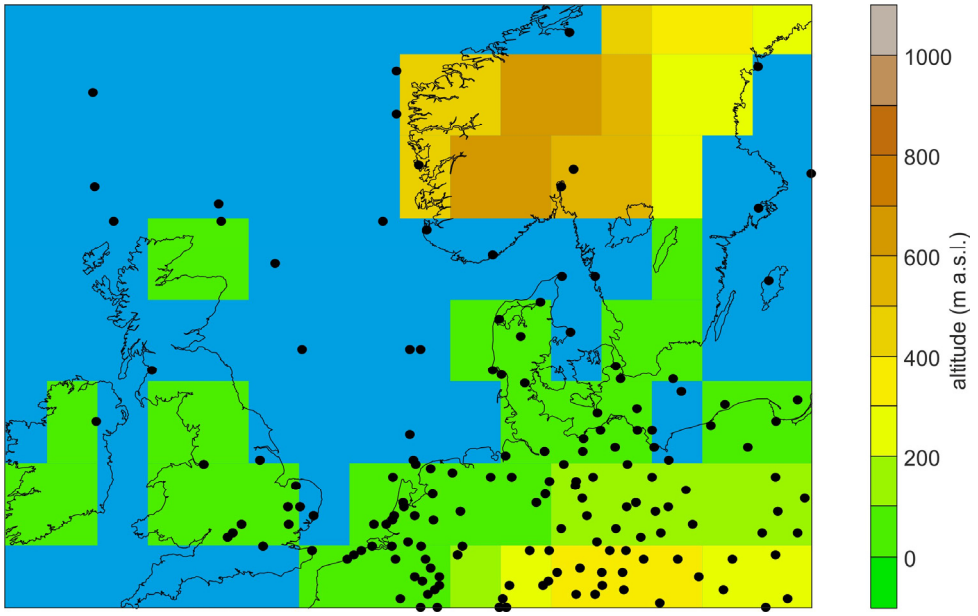

Figure 2. Map showing the surface and sea-level pressure measurements assimilated into 20CR on 31 January 1953, 12 UTC. Colours indicate the orography in 20CR and the land-sea mask as depicted in the Gaussian grid (192 x 94 cells).

2011). 20CR is a new, global six-hourly reanalysis that reaches back to 1871. The goal of this paper is to analyse the 1953 Holland storm in 20CR and to compare the findings with results from other authors using other data sets.

This paper is organized as follows. Section 2 describes the data and methods used. The meteorological situation as depicted in 20CR is presented in Section 3. In Section 4 results are discussed and compared with other data sets. Finally, conclusions are drawn in Section 5.

2. Data and Methods

This study makes use of the second version of the "Twentieth Century Reanalysis" (20CR, Compo et al., 2011), covering the period 1871-2010. 20CR assimilates observations of surface and sea-level pressure into the NCEP/CFS forecasting model using a variant of the Ensemble Kalman Filter. The model is forced by monthly sea-surface temperatures and sea ice distribution and is run at a spectral truncation of T62 (corresponding to a horizontal resolution of 2° x 2°) and 28 levels in the vertical. Figure 2 shows the air pressure data assimilated into 20CR for the analysis on 31 January 1953, 12 UTC. Also shown is the orography of 20CR and the land sea mask. 20CR provides analyses every six hours and is the first estimate of the global state of the atmosphere back to the 19th century from reanalysis efforts. 20CR consists of a 56 member ensemble; however, in this paper we use mostly only the ensemble mean.

In this study, we focus on the variables sea-level pressure (SLP), geopotential height (GPH), 10 m wind speed, and ensemble mean *u* and *v* wind components at upper levels. 20CR is compared to historical SLP analyses from the German Hydrographical Institute (Deutsches Hydrographisches Institut, 1966) and from Rossiter (1954). For assessing wind speed we consult estimates and measurements for the coast of the Netherlands as found in Lamb (1991)

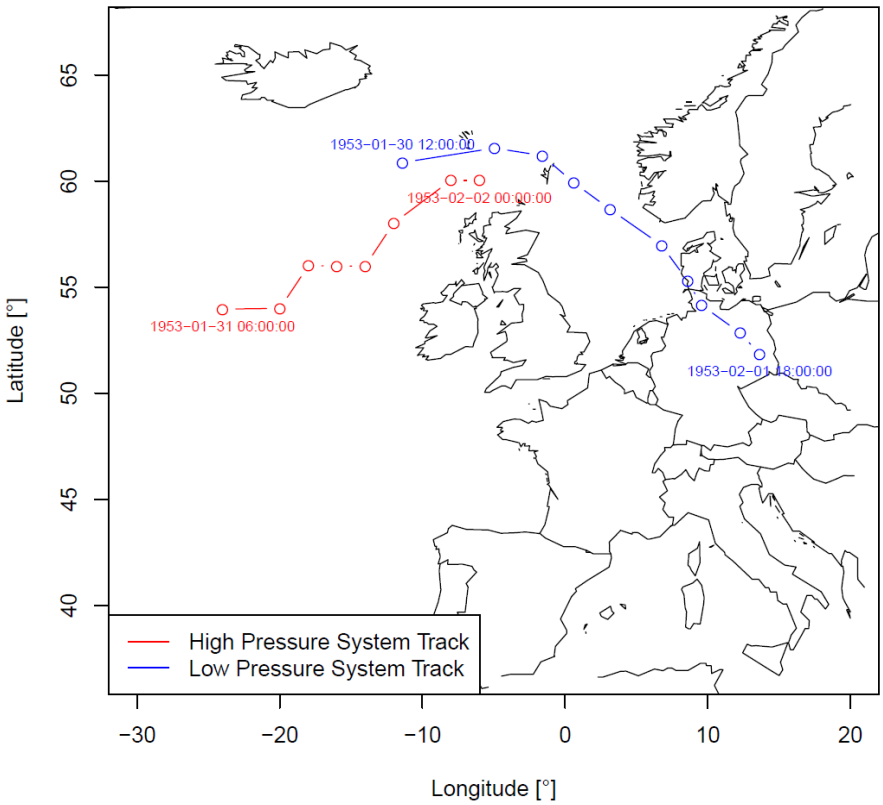

Figure 3. Track of the high/low pressure systems (red/blue) in the SLP field.

and in ECA&D data (Klein Tank et al. 2002). Additionally, we compare 20CR with EMULATE SLP data (Ansell et al., 2006) and with other reanalysis products, including a reanalysis using the ECMWF system (IFS) at a high resolution (T511) (Jung et al., 2004), NCEP/NCAR reanalysis (Kistler et al., 2001), and radiosonde observations from CHUAN (Stickler et al., 2010).

Finally, data of tide height and information about the water level at the coast have been consulted. For the period 31 January 1953, 0 UTC, to 2 February, 0 UTC, hourly tide heights of the following stations are plotted: Oostende (Belgium), Brouwershavn, Ijmuiden, Harlingen (all Netherlands) and Borkum (Germany). The observations are extracted from Rossiter (1954).

3. Results from 20CR

From 30 January to 2 February 1953, a surface low pressure system related to an upper-tropospheric ridge-trough pattern moved across the North Atlantic. The low pressure system moved from the Faroe Islands in easterly direction until midnight 31 January when it turned to south-easterly direction and into the German Bight towards Hamburg. On 31 January the pressure of this cyclone was reaching an absolute minimum below 980 hPa (ensemble mean). To the west of the low pressure system, a pronounced high-pressure system was observed over the Atlantic, leading to strong pressure gradients. The high pressure system moved from its initial position west of Ireland to the Faroe Islands. Figure 3 shows the tracks of the two systems in the SLP field of 20CR, calculated in the same way as in Neff et al. (this issue), but based on the ensemble mean. SLP and 200 hPa GPH on 1 February 0 UTC, just before the

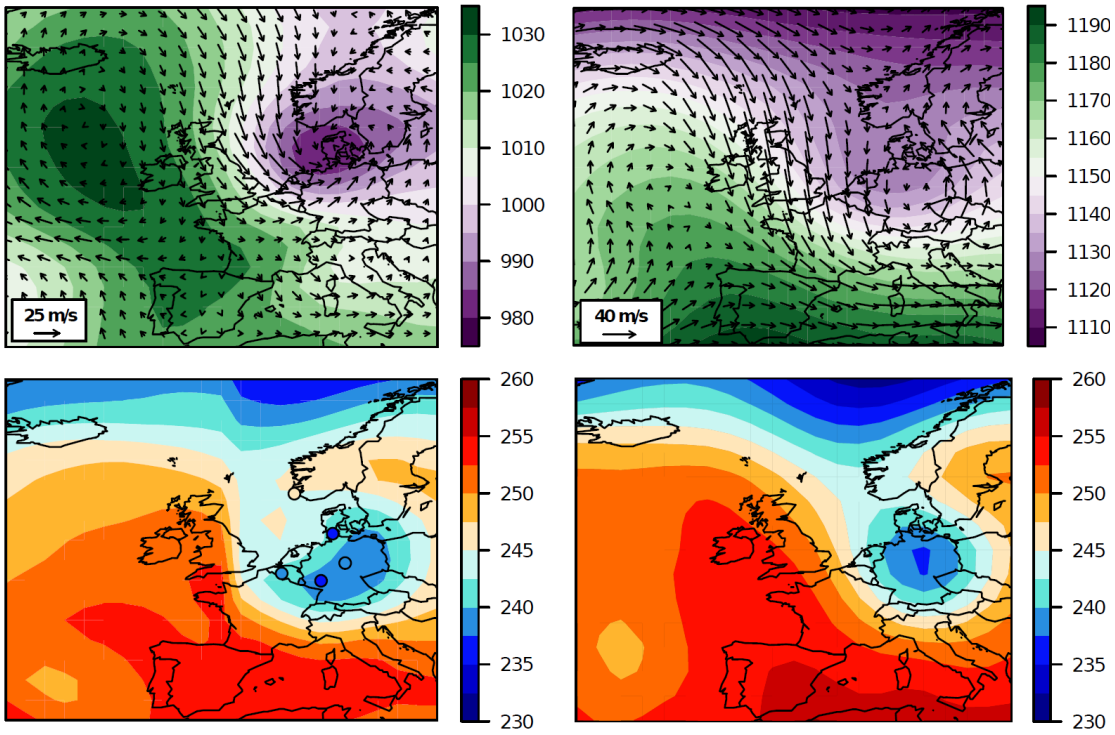

Figure 4. The meteorological situation on 1 February 1953, 0 UTC, almost at the peak of the event: (top left) sea-level pressure and 10 m wind from 20CR, (top right) geopotential height (gpdm) and wind at 200 hPa from 20CR, (bottom left) 500 hPa temperature from 20CR and (bottom right) 500 hPa temperature from NCEP/NCAR. Dots in the bottom left figure denote temperature observations from CHUAN radiosonde data in the vicinity of the cold air.

peak sea level at 3 UTC, are shown in Figure 4. The SLP figure shows the strengths of both pressure systems, with a difference of more than 50 hPa over a distance of about 1750 km. The strong pressure gradient throughout the troposphere between Ireland and Denmark/Northern Germany resulted in high wind speeds over the North Sea. Northerly to north-westerly winds in 20CR (ensemble mean) exceed speeds of 30 m/s on 1 February, 0 UTC. The ridge-trough pattern is clearly visible at the 200 hPa level, with northerly and northwesterly winds. In addition, 500 hPa temperatures from 20CR (Fig. 4, bottom left) show the inflow of cold air towards central Europe in the middle troposphere. Temperature differences of up to 15 K are found between Germany and England.

4. Discussion and comparison to other data sets

The results from 20CR fit well with previous analyses based on other data sources. Rossiter (1954) describes a deepening cyclone on 30 January, moving from the northern Atlantic in south-easterly direction (Rossiter, 1954). When the low pressure system developed south of Iceland, the weather situation appeared rather harmless to forecasters (Deutsches Hydrographisches Institut, 1966). The cyclone reached northern Scotland on 31 January, 0 UTC. However, low pressure systems approaching the north of Scotland and travelling eastward do generally not veer into the North Sea but tend to pass toward Scandinavia (Rossiter, 1954). In this case the cold polar air (see Fig. 4) flowing south-eastward in higher atmospheric layers, together with the approaching high pressure system, guided the cyclone into the North Sea (Rossiter, 1954). When the cyclone reached the North Sea at noon of 31

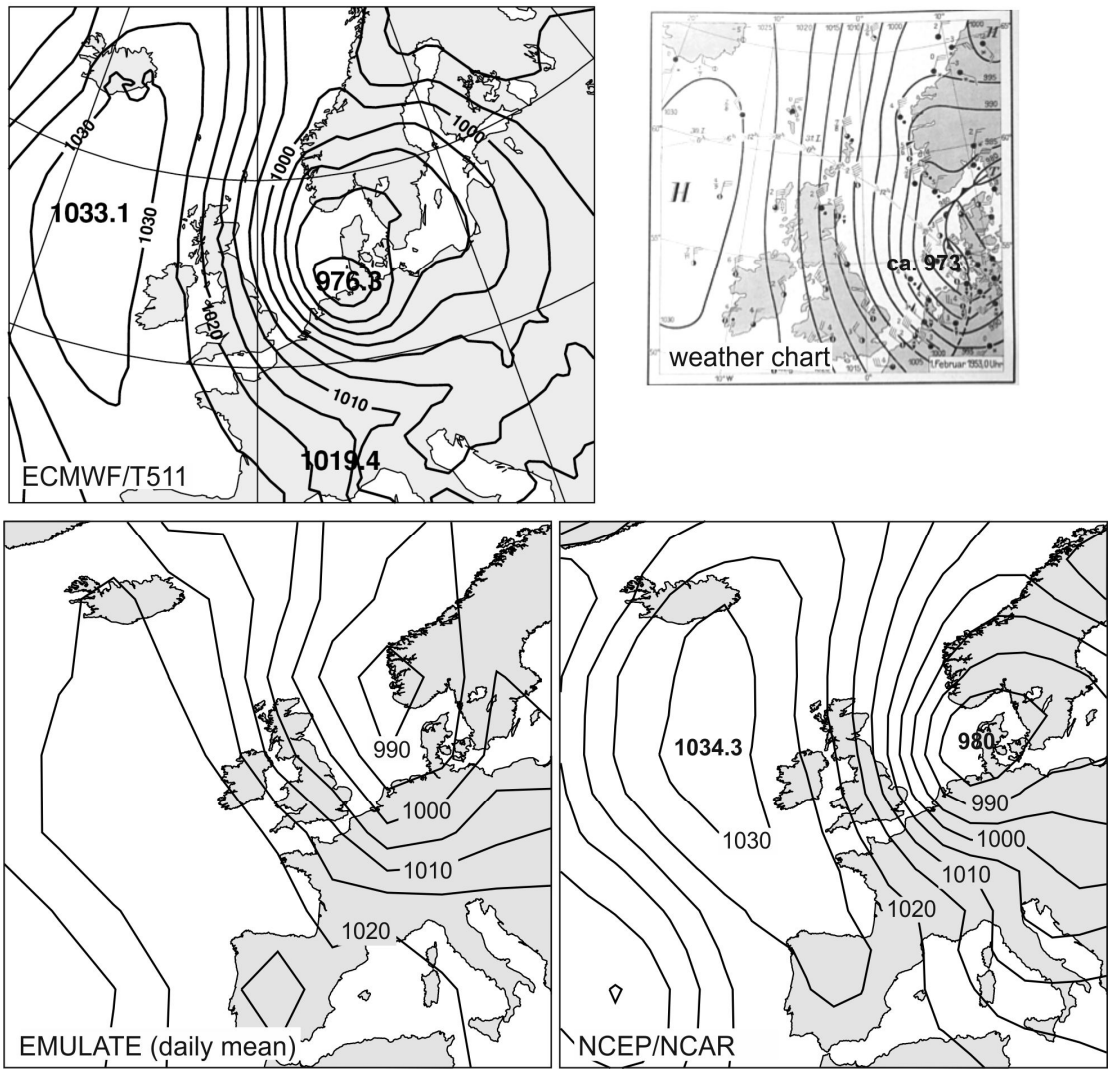

Figure 5. SLP (hPa) on 1 February 1953, 0 UTC, in (top left) the reanalysis performed with the ECMWF high-resolution system (T511) (from Jung et al., 2004, copyright © 2004 Royal Meteorological Society, reprinted with permission), (top right) the historical hand-analysed chart (Deutsches Hydrographisches Institut, 1966), (bottom left) EMULATE daily SLP field for 1 February 1953 and (bottom right) NCEP/NCAR reanalysis. The corresponding field from 20CR (min: 980 hPa, max: 1031.8 hPa) is shown in Fig. 4.

January, it also reached its lowest central pressure. Then the low pressure system moved eastward into the German Bight.

The development of the cyclone, as described in the abundant literature, is well depicted in 20CR. To further assess 20CR we compared individual fields with other data sources. SLP data were compared with historical analyses, NCEP/NCAR reanalysis, EMULATE SLP data, as well as with the ECMWF high-resolution reanalysis (Figures taken from Jung et al., 2004) in Figure 5. The results show that 20CR (Fig. 4, top left) provides a realistic depiction of the cyclone even in the ensemble mean, although the minimum pressure is slightly higher than in the hand-analysed fields and in the high-resolution reanalysis of ECMWF (Jung et al., 2004). 20CR shows very similar extreme values (in the ensemble mean) as the NCEP/NCAR reanalysis, while the EMULATE SLP field (note that the latter are daily averages) shows considerably weaker extremes.

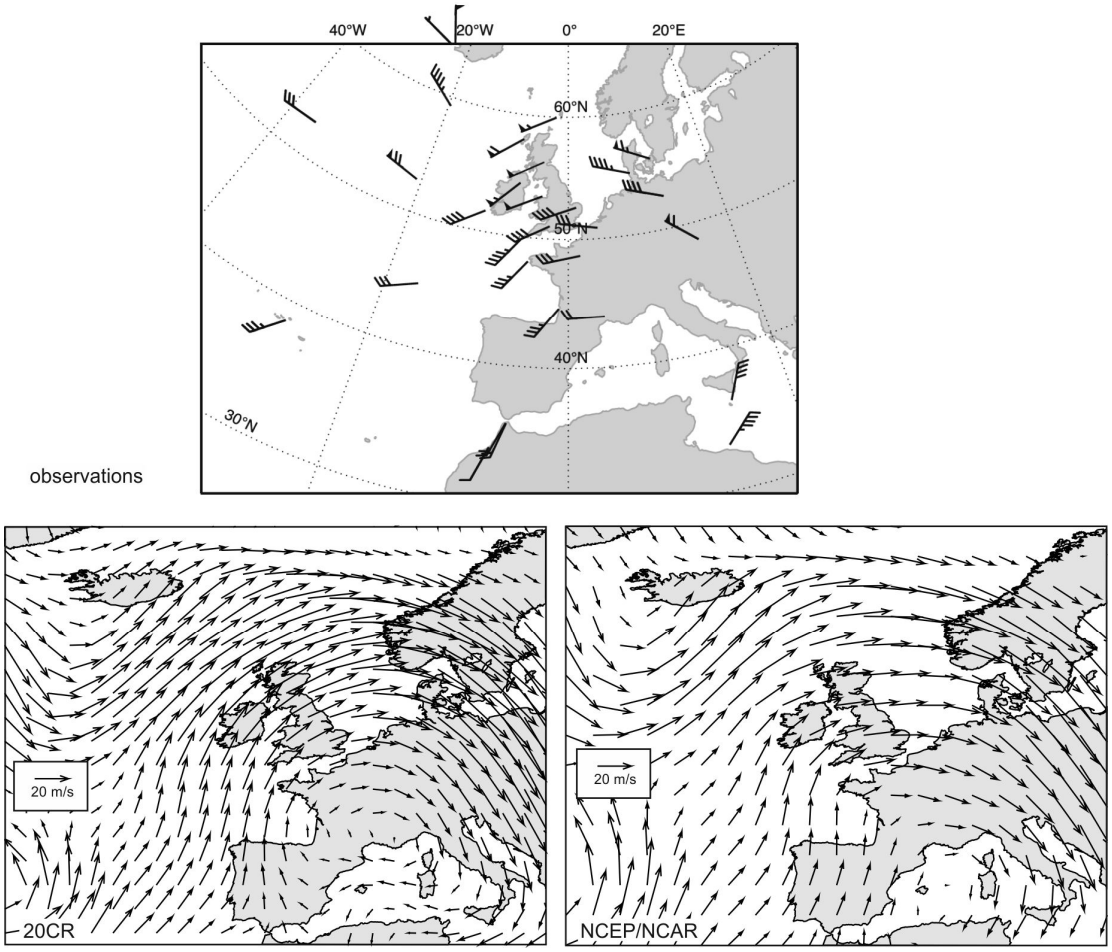

Figure 6. Wind at 500 hPa on 30 January 1953 in (top) radiosonde observations between 10-15 UTC (from Jung et al. 2004, copyright © 2004 Royal Meteorological Society, reprinted with permission), (bottom left) 20CR at 12 UTC, and (bottom right) NCEP/NCAR at 12 UTC.

Figure 6 shows a similar comparison for 500 hPa winds, two days earlier. The figure displaying observations is taken from Jung et al. (2004). Over Europe, both 20CR and NCEP/NCAR reanalyses fit very well with the observations, but over the Atlantic a discrepancy arises southwest of Iceland, where observations indicate westerly or northwesterly winds but both reanalyses show southwesterlies.

Temperatures at 500 hPa in 20CR on 30 January fit well with NCEP/NCAR reanalyses and with CHUAN radiosonde observations in the vicinity of the cold air (Fig. 4, bottom). Note that the latter have been assimilated into NCEP/NCAR, but not into 20CR.

Surface wind speeds in 20CR are compared to scattered quotes in the literature. Lamb (1991) calculated maximum gradient wind speeds from the SLP for 31 January to 1 February 1953, ranging from 100-130 knots (51 to 66 m/s). The daily average wind speed at the station in Den Helder at the Dutch coast is reported as 20.1 m/s in ECA&D. The main reason for the difference between these two wind speeds might be due to friction as surface roughness is not taken into account in the calculated gradient wind. In 20CR, 10 m wind speed around Den Helder reaches 22.5 m/s in the ensemble mean. This is in very good agreement with observations.

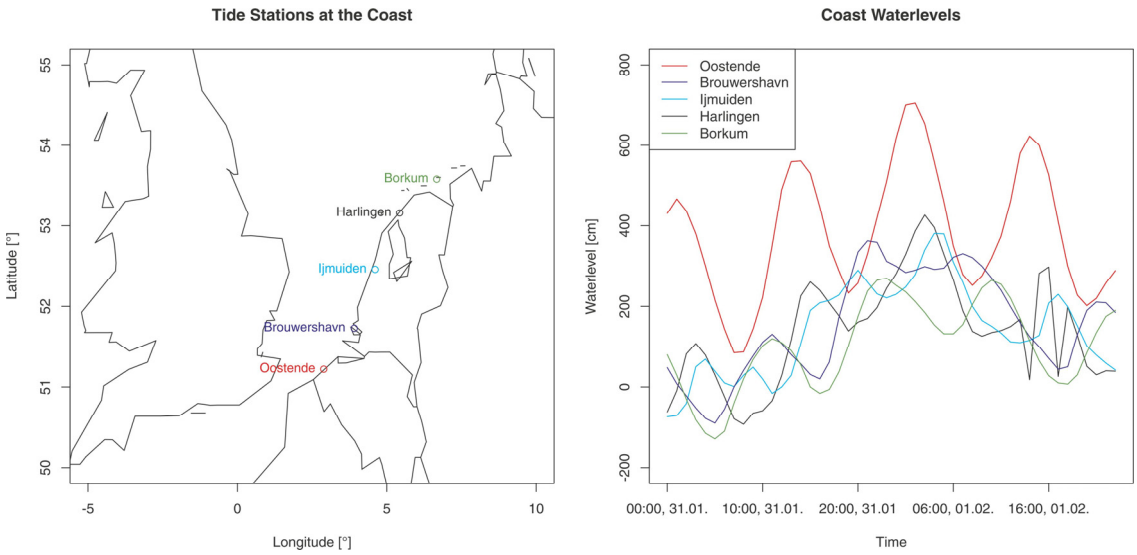

Figure 7. The tide stations display the used tidal data. The water levels are increasing in all stations until 1 February at 3:00 UTC. Oostende shows the highest values due to the tailback effect of the Strait of Dover.

Finally, we analysed historical tide data (although 20CR does not contain information on waves and sea level) because coastal protection is an important further application of products such as 20CR. We used tide data from observations, taken from Rossiter (1954). Figure 7a shows tide stations in the affected area. From midnight 31 January on, a rapid rise of water levels of all stations is measured (Fig. 7b). The water level peaked at 3 UTC on 1 February which lags the wind speed maxima by a few hours. The highest water levels were registered in Oostende, Ijmuiden and Harlingen with a small delay due to tidal shift. Brouwershavn is lying in the backwaters instead of the coast as the other stations, which explains that the curve fluctuates less in between the tides. The station Oostende shows the highest water levels which results from the tailback effect of the Strait of Dover (Rossiter, 1954). The important factor here is the accumulation of the surge due to the narrowing of the strait. According to Hansen (1956) extremely high water levels in shallow water areas react very rapidly to changes in local winds. Additionally, the funnel-shaped river mouths of the Netherlands also enforced tailback effects which increased water levels.

5. Conclusion

Several factors led to the extreme storm surge in Holland in 1953, most notably the combination of a storm, an accumulation of the large surge in the Strait of Dover, and high spring tide (Hansen, 1956). Sustained high northerly wind speeds due to a strong cyclone pushed water masses southward in the North Sea, and a long fetch allowed for the development of large wind induced waves (Wolf and Flather, 2005). Much of the area affected was below sea level and the dykes could not prevent their flooding.

The analysis of 20CR and other data sets showed that 20CR is in good agreement with other data sources and with previous meteorological interpretations of the event. Thus, at least for this storm event, 20CR is a suitable data set.

Acknowledgement

The work was funded by the EC FP7 project ERA-CLIM and by the Swiss National Science Foundation project EVALUATE. 20CR data were provided by courtesy of the NOAA/OAR/ESRL PSD, 131 Boulder, Colorado, USA (http://www.esrl.noaa.gov/psd/). Support for the Twentieth Century Reanalysis Project dataset is provided by the U.S. Department of Energy, Office of Science Innovative and Novel Computational Impact on Theory and Experiment (DOE INCITE) program, and Office of Biological and Environmental Research (BER), and by the National Oceanic and Atmospheric Administration Climate Program Office. We also acknowledge data provided by ECA&D.

References

Ansell, T. J., P. D. Jones, R. J. Allan, D. Lister, D.E. Parker, M. Brunet, A. Moberg, J. Jacobeit, P. Brohan, N. A. Rayner, E. Aguilar, M. Barriendos, T. Brandsma, N. J. Cox, P. M. Della-Marta, A. Drebs, D. Founda, F. Gerstengarbe, K. Hickey, T. Jónsson, J. Luterbacher, Ø. Nordli, H. Oesterle, M. Petrakis, A. Philipp, M. J. Rodwell, O. Saladie, J. Sigro, V. Slonosky, L. Srnec, V. Swail, A. M. García-Suárez, H. Tuomenvirta, X. Wang, H. Wanner, P. Werner, D. Wheeler, and E. Xoplaki (2006) Daily mean sea level pressure reconstructions for the European-North Atlantic region for the period 1850–2003. *J. Climate,* **19,** 2717–2742.

Compo, G. P., J. S. Whitaker, P. D. Sardeshmukh, N. Matsui, R. J. Allan, X. Yin, B. E. Gleason, R. S. Vose, G. Rutledge, P. Bessemoulin, S. Brönnimann, M. Brunet, R. I. Crouthamel, A. N. Grant, P. Y. Groisman, P. D. Jones, M. C. Kruk, A. C. Kruger, G. J. Marshall, M. Maugeri, H. Y. Mok, Ø. Nordli, T. F. Ross, R. M. Trigo, X. L. Wang, S. D. Woodruff, and S. J. Worley (2011) The Twentieth Century Reanalysis project. *Q. J. Roy. Meteorol. Soc.,* **137**, 1-28.

Deutsches Hydrographisches Institut (1966) *Nordsee Handbuch. Östlicher Teil.* Deutsches Hydrographisches Institut, Hamburg. 566 pp.

Gerritsen, H. (2005) What happened in 1953? The Big Flood in the Netherlands in retrospect. *Phil. Trans. R. Soc. A,* **363,** 1271–1291.

Hansen, W. (1956) Theorie zur Errechnung des Wasserstandes und der Strömungen in Randmeeren nebst Anwendungen. *Tellus,* **8,** 287–300.

Jung, T., E. Klinker, and S. Uppala, S. (2004) Reanalysis and reforecast of three major European storms of the twentieth century using the ECMWF forecasting system. Part I: Analyses and deterministic forecasts. *Meteorol. Appl.* **11,** 343–361.

Kistler, R., E. Kalnay, W. Collins, S. Saha, G. White, J. Woollen, M. Chelliah, W. Ebisuzaki, M. Kanamitsu, V. Kousky, H. van den Dool, R. Jenne, and M. Fiorino (2001) The NCEP–NCAR 50-Year Reanalysis: Monthly Means CD-ROM and Documentation. *Bull. Am. Meteorol. Soc.,* **82,** 247-267.

Klein Tank, A. M. G., J. B. Wijngaard, G. P. Können, R. Böhm, G. Demarée, A. Gocheva, M. Mileta, S. Pashiardis, L. Hejkrlik, C. Kern-Hansen, R. Heino, P. Bessemoulin, G. Müller-Westermeier, M. Tzanakou, S. Szalai, T. Pálsdóttir, D. Fitzgerald, S. Rubin, M. Capaldo, M. Maugeri, A. Leitass, A. Bukantis, R. Aberfeld, A. F. V. van Engelen, E. Forland, M. Mietus, F. Coelho, C. Mares, V. Razuvaev, E. Nieplova, T. Cegnar, J. Antonio López, B. Dahlström, A. Moberg, W. Kirchhofer, A. Ceylan, O. Pachaliuk, L. V. Alexander, P. Petrovic (2002) Daily dataset of 20th-century surface air temperature and precipitation series for the European Climate Assessment. *Int. J. of Climatol.,* **22,** 1441-1453.

Lamb, H. H. (1991) *Historic storms of the North Sea, British Isles, and Northwest Europe.* Cambridge University Print, Cambridge, 204 pp.

McRobie, A., T. Spencer, and H. Gerritsen (2005) The big flood: North Sea storm surge. *Phil. Trans. R. Soc. A,* **363,** 1263–1270.

Neff, B., C. Kummli, A. Stickler, J. Franke, and S. Brönnimann (2013) An analysis of the Galveston Hurricane using the 20CR data set. In: Brönnimann, S. and O. Martius (Eds.) *Weather extremes during the past 140 years*. Geographica Bernensia G89, p. 27-34, DOI: 104480/GB2013.G89.03.

Rossiter, J. R. (1954) The North Sea storm surge of 31 January and 1 February 1953. *Phil. Trans. R. Soc. A,* **246,** 371–400.

Smits, A., A. M. G. Klein Tank, and G. P. Können (2005). Trends in storminess over the Netherlands, 1962–2002. *Int. J. Climatol.,* **25,** 1331–1344.

Stickler, A., A. N. Grant, T. Ewen, T. F. Ross, R. S. Vose, J. Comeaux, P. Bessemoulin, K. Jylhä, W. K. Adam, P. Jeannet, A. Nagurny, A. M. Sterin, R. Allan, G. P. Compo, T. Griesser, and S. Brönnimann (2010) The comprehensive historical upper-air network. *Bull. Amer. Meteorol. Soc.,* **91,** 741-751.

Verlaan, M., A. Zijderveld, H. de Vries, and J. Kroos (2005) Operational storm surge forecasting in the Netherlands: developments in the last decade. *Phil. Trans. R. Soc. A,* **363,** 1441–1453.

Wolf, J. and R. A. Flather (2005). Modelling waves and surges during the 1953 storm. *Phil. Trans. R. Soc. A,* **363,** 1359–1375.